applied sciences

MDPI

Article

Experimental and Numerical Investigations on Curing a Polyester-Based Powder Coating by Catalytic Infrared Radiation

Yindong Yuan [1], Song Pan [1], Tongzhao Wang [2,*], Liang Xia [2], Yiqiao Liu [3], Xinru Wang [4], Lei Li [5] and Tian Wang [2]

[1] Beijing Key Laboratory of Green Built Environment and Efficient Technology, Beijing University of Technology, Beijing 100124, China
[2] Department of Architecture and Built Environment, Research Centre for Fluids and Thermal Engineering, University of Nottingham Ningbo China, Ningbo 315100, China
[3] Department of Mechanical Engineering, Faculty of Engineering, Universiti Malaya, Kuala Lumpur 50603, Malaysia
[4] College of Mechanical Engineering, Tianjin University of Commerce, Tianjin 300134, China
[5] Suzhou Catalytic Green Energy Co., Ltd., Suzhou 215011, China
* Correspondence: tongzhao.wang@nottingham.edu.cn; Tel.: +86-13863390016

Abstract: Catalytic combustion can effectively and cleanly convert the chemical energy of fossil fuels into infrared radiation energy. However, there is little research on the use of this technology to cure powder coatings. Therefore, catalytic infrared heating equipment based on a Pt/Al_2O_3 noble metal catalyst was designed, constructed, and tested in this study. The optimal curing parameters for the catalytic infrared curing process for powder coatings were determined via experiments at 220 °C for 3 min and 230 °C for 2 min. As the curing temperature increased and the curing time increased, the mechanical properties of the coating were found to improve. However, the gloss of the coating was reduced and the color darkened. A one-dimensional heat transfer model was developed to investigate the heat transfer process for powder coatings. This study introduced an internal heat source for the first time, and the heat transfer process for polyester-based powder coatings with different substrate thicknesses was numerically simulated. The numerical simulations demonstrated that the efficiency of the heat transfer between the catalytic infrared gas supply and the coating surface was 0.4. When the substrate thickness was 1 mm, the coating was most rapidly cured at 230 °C. When the substrate thickness was ≥2 mm, the most rapid curing occurred at 220 °C.

Keywords: catalytic infrared; heat efficiency; heat transfer model; powder coating curing

check for updates

Citation: Yuan, Y.; Pan, S.; Wang, T.; Xia, L.; Liu, Y.; Wang, X.; Li, L.; Wang, T. Experimental and Numerical Investigations on Curing a Polyester-Based Powder Coating by Catalytic Infrared Radiation. *Appl. Sci.* **2023**, *13*, 2187. https://doi.org/10.3390/app13042187

Academic Editor: Eric Guibal

Received: 16 November 2022
Revised: 23 January 2023
Accepted: 6 February 2023
Published: 8 February 2023

Copyright: © 2023 by the authors. Licensee MDPI, Basel, Switzerland. This article is an open access article distributed under the terms and conditions of the Creative Commons Attribution (CC BY) license (https://creativecommons.org/licenses/by/4.0/).

1. Introduction

Powder coatings on metal surfaces and other materials can be used for protection, decoration, and other special functions. These coatings are widely used in the automobile, aerospace, machinery, and furniture industries, as well as others [1–4]. However, for metal substrates, adequate protection is only possible if the coating remains bonded to the substrate for the design life of the metal structure and has excellent mechanical properties. The mechanical properties of the coating are usually tested in terms of adhesion, hardness, and impact resistance. In addition to ensuring the mechanical properties of the coating are appropriate, the aesthetic effect of the coating is significant. A natural and attractive appearance increases consumer satisfaction [5]. Gloss and color tests are usually performed to evaluate the gloss and color difference in cured coatings.

ChuanXing Wang et al. [6] used a hot-air curing oven at 180 °C for 10 min to cure a two-layer powder coating. Furthermore, they investigated the effects of two curing strategies—co-curing and layer-by-layer curing—on the mechanical properties of the coating. The results showed that the coatings' adhesion, gloss, and hardness were higher with the layer-by-layer curing than those

obtained with the co-curing mode. M. Puig et al. [7] cured polyester-based powder coatings with different organo-modified silica particle (OSP) concentrations (1, 2.5, 3.5, and 4.5 wt.%) using a hot air method at 180 °C for 15 min. Then, they tested the samples with different OSP concentrations for adhesion and impact resistance. The results showed that the samples with a 2.5% OSP concentration had improved adhesion and impact resistance. Jingwen Zhang et al. [8] used a hot-air curing oven to cure epoxy powder (EP) coatings with a graphene nanosheet (G) added at 210 °C for 10 min, and the adhesion and impact resistance of the cured composite (G/EP) coating and EP samples were tested. The results confirmed that the G/EP coating could significantly improve adhesion and impact resistance compared to the EP coating. Jiang Rong et al. [9] used a hot-air curing oven to cure powder coatings and studied the effect of curing temperature and curing time on the gloss of the powder coatings. The results showed that the coating gloss decreased to a great extent as the curing temperature and time increased. Suresh et al. [10] used ultraviolet light to cure coatings at different temperatures and found that the gloss of the coatings decreased more at higher temperatures. R. Knischka et al. [11] studied the color change in cured coatings with different near-infrared absorber (NIR-A) addition levels. They found that the coatings' a* and b* values decreased with increasing levels of NIR-A addition.

According to the literature review, the mechanical properties and appearance of coatings are influenced by the their components. The curing temperature and time are also very important for the coating curing quality. In addition, most recent studies use hot-air ovens to cure powder coatings with curing times of 10–15 min, which undoubtedly increases the time required for the process and the energy consumption. As the output requires a conveyor device to ensure the continuity of production, longer curing times increase the length of the production line.

Selecting the appropriate curing procedure helps to ensure high coating quality while conserving energy. It is currently difficult to achieve high-efficiency and low-energy mass production with conventional convection curing processes. Nevertheless, in recent decades, infrared heating technology and heat radiation systems have been significantly improved. Kyung Jae Park et al. [12] applied an infrared oven system to a continuous coil coating line. Their results indicated that the quality of the products obtained with the infrared oven was better than with a traditional hot-air oven, and the energy consumption was reduced by approximately 30%. L. Véchot et al. [13] used an infrared heating system to rapidly cure a polyester-based powder coating. Near-infrared (NIR) heating technology is widely used in the coating industry due to its high energy density and fast curing ability [14,15].

Catalytic infrared radiation is energy in the form of electromagnetic waves, which are generated from the reaction of natural gas with oxygen under the action of a catalyst. Catalytic infrared radiation has resulted in remarkable achievements in the dried food industry [16–18]. However, to the best of our knowledge, the properties and primary experimental data for catalytic infrared curing of powder coatings have not yet been reported. The application of catalytic infrared technology for powder coating curing has the following potential advantages [19–22]:

- Catalytic infrared heating equipment predominantly produces mid-wave and long-wave infrared radiation. This matches the spectral absorption characteristics of powder coatings, accelerating the curing process;
- Catalytic infrared technology directly converts gas into infrared radiation under the action of a catalyst, resulting in higher energy conversion efficiency. The conversion rate for methane, the main component of natural gas, can reach more than 98%;
- Catalytic combustion releases infrared radiation energy, enabling the efficient and complete combustion of gas at low temperatures. Low-temperature (<600 °C) combustion reduces the generation of polluting gases, such as CO and NOx. Lower pollutant emissions can be obtained (~5 ppm compared to 150–200 ppm with conventional combustion) [21]. It is assumed that only CO_2 and H_2O are produced [23].

Therefore, employing catalytic infrared technology for the curing of powder coatings has important research significance and good potential for application in engineering.

Changes in the coating temperature during curing impact the coating quality. Numerical simulation is an effective strategy for the visualization of heat transfer behavior in curing processes and their performance. Studies have used numerical simulation methods to investigate the thermal behavior of a drying process [24], an air conditioning plant paint-curing oven [25], a cranberry-drying process [26], a potato slice-drying process [27], and a household toast grill [28]. With regard to powder coating curing, L. Véchot and I. Bombard et al. coupled thermal simulations and curing process dynamics to develop a model for the prediction of the evolution of the coating temperature and the degree of conversion under electric infrared radiation [13,29]. However, no model has yet been reported for the prediction of the temperature changes in coatings under catalytic infrared radiation.

Accordingly, this work aimed to study the influence of catalytic infrared treatment on coating quality under different heating conditions. The quality of the cured coatings under different conditions was evaluated in terms of adhesion, gloss, hardness, impact resistance, and color. The best curing parameters for a polyester-based powder coating were obtained, and a model was established for the prediction of the temperature changes in this powder coating with catalytic infrared heating. This work is expected to serve as a guide for the production of powder coatings and the design of catalytic infrared systems and may help improve the efficiency and energy savings of catalytic infrared heating systems. To clearly describe the work and the steps in this study, the research framework is shown in Figure 1.

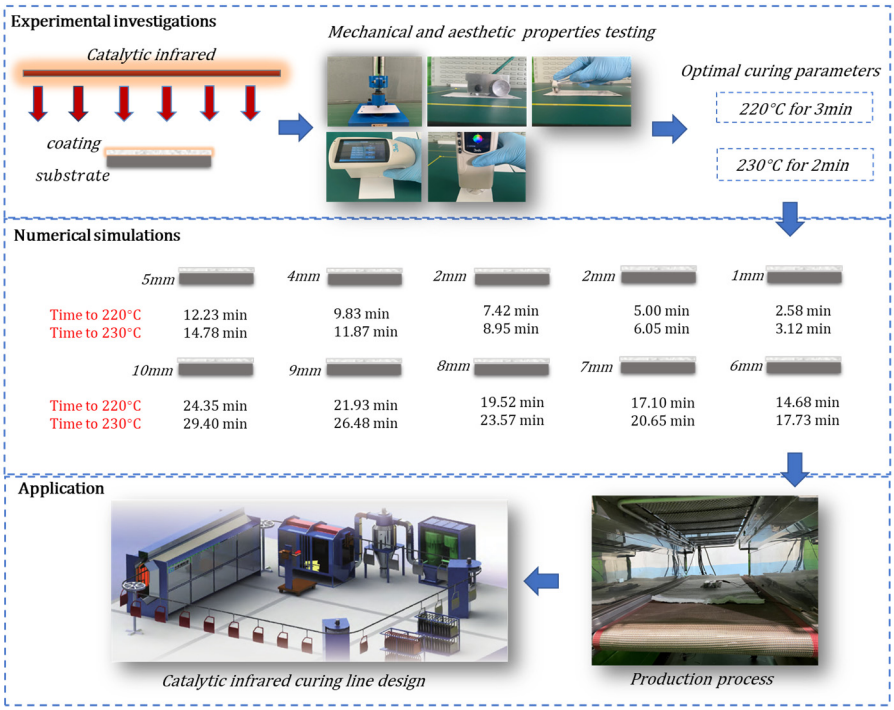


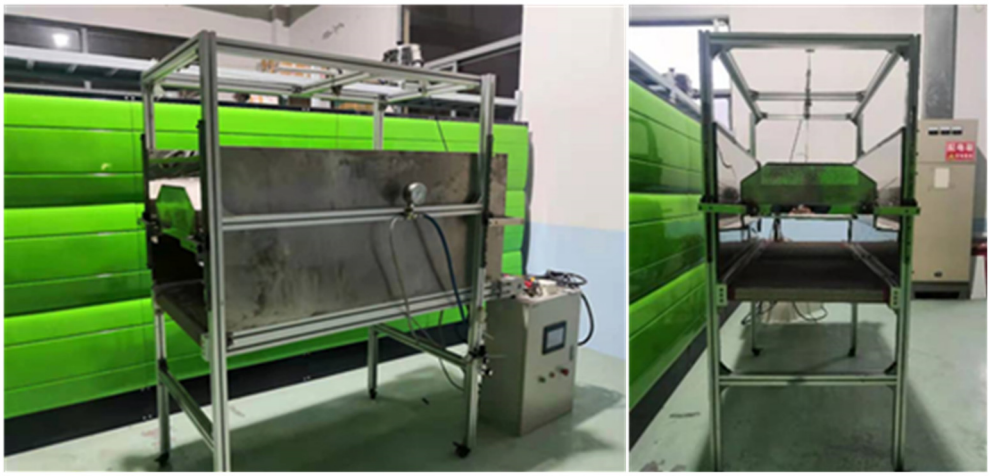
Figure 1. Research framework.

2. Experimental Investigations

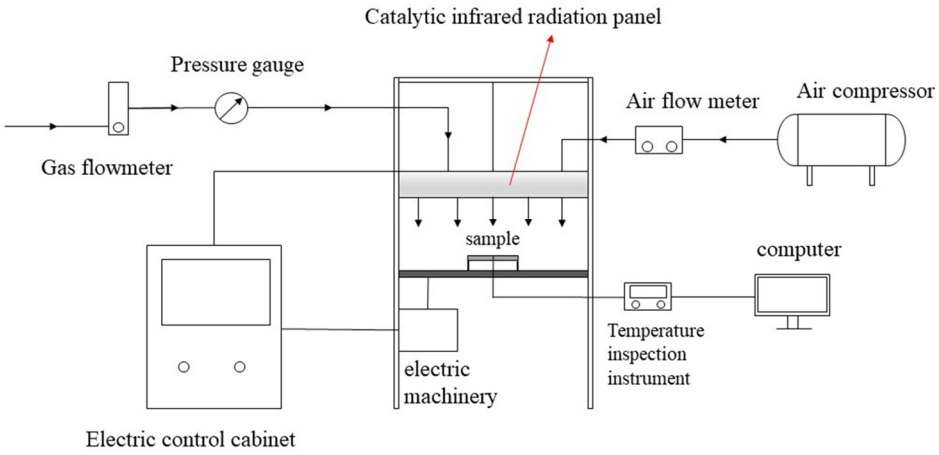
2.1. Equipment and Materials

A catalytic infrared equipment setup was constructed, including a catalytic infrared radiator system, a gas supply system, an electric control system, a temperature measurement system, and the main body of the equipment, as displayed in Figure 2. The radiation plate (800 × 400 × 50 mm) used in the experiment is shown in Figure 3, and its maximum power was 4 kW. Two catalytic infrared radiation panels were located on top of the equipment. The bottom platform was insulated and equipped with a base frame to prevent heat transfer between the coating sample and the platform. A control cabinet was used to adjust the distance between the radiation panels and the sample. During the curing process, the samples' temperatures and the air inside the equipment were measured using

K-type thermocouples. We set one temperature measurement point centered at the top of the samples and one centered at the bottom. The temperature signals were transmitted to a computer. A portable infrared thermometer was used to measure the temperature at the panel's surface in real time. The gas used in this experiment was liquefied petroleum gas (LPG) from a tank. The details of the experimental instruments are shown in Table 1.



(**a**)



(**b**)

Figure 2. (**a**) Catalytic infrared curing oven. (**b**) Schematic diagram of infrared curing furnace with catalytic combustion.

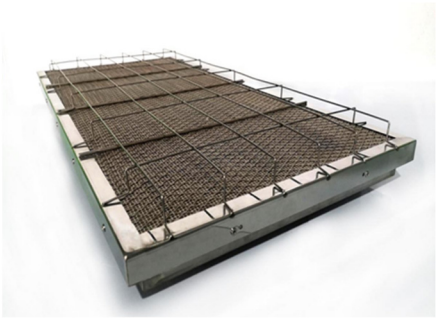


Figure 3. Catalytic infrared radiation panel.

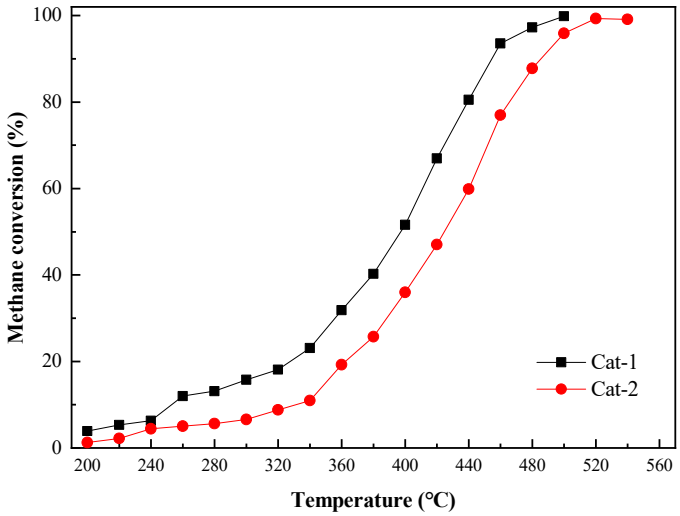
Table 1. Details of the experimental instruments.

Name	Picture	Model	Range	Precision	Error
K-Type thermocouple		WRNT-01	−200~500 °C	0.1	0.5%
Temperature logger		KCM-LCD16	−30~1300 °C	0.1	-
Infrared thermometer		MS Plus	−32~530 °C	0.1	1%
Gloss meter		HG60	0~300 GU	0.1	0.2%
Universal colorimeter		NR10QC	L* 0–100 a*, b* −100–100	0.01	0.03%

The catalyst used in this study was prepared using high-temperature calcination with fibrous alumina as the carrier and platinum and other trace metal components, as shown in Figure 4a. The characteristics of this catalyst are summarized in Table 2. The changes in the methane conversion rate with temperature under the action of the catalyst provided by Suzhou Catalytic Green Energy Co., Ltd. (Suzhou, China) are shown in Figure 4b. The Cat-1 catalyst exhibited a more effective ability to transform methane than the Cat-2 catalyst, so Cat-1 was used in this study.



(**a**)



(**b**)

Figure 4. (**a**) Fiber-supported noble metal catalyst. (**b**) Methane conversion versus temperature with the Cat-1 and Cat-2 catalysts.

Table 2. Physical properties of fiber-supported noble metal catalyst (Cat-1).

Index	Value	Unit
Dimensions	745 × 395 × 5	mm
Catalyst loading per area	350	g/m^2
Average diameter	5	μm
Average particle size	18	nm
Specific surface area	150	m^2/g
Pore volume	0.14	cm^3/g
Average pore size	5.25	nm
Elemental content	Pt ≤ 1 wt.%, Al_2O_3 ≥ 95 wt.%, SiO_2 ≤ 4 wt.%	/
Ignition temperature	120 (LPG), 180 (natural gas)	°C
Service life	30,000	h

The powder coating used in this study was a triglycidyl isocyanurate (TGIC) polyester system (provided by Jiangsu Aiyue Powder Coating Co., Ltd., Taicang, China), which is widely used in the metal coating industry. The characteristics of this powder coating are summarized in Table 3. The substrates were test-grade galvanized steel panels, and the size of these plates was 150 × 70 × 1 mm. The powder coating was sprayed with a high-voltage electrostatic spray gun, and the thickness of the paint film was controlled at 100 μm.

Table 3. Characteristics of the powder coating used in this study.

Index	Parameter
Composition	Polyester-based powder coating + triglycidylisocyanurate crosslinker, acrylic acid, barium sulfate, titanium dioxide, pigments, and various additives
Average particle size	34–38 μm
Color	White
Thermal conductivity (average)	0.1 W/m·°C
Glass transition temperature	53 °C
Curing conditions (hot-air oven)	200 °C for 10 min and 180 °C for 20 min
Storage stability	Below 25 °C; the storage time was 12 months

2.2. Experimental Setup

This work aimed to determine the radiant heating performance of a catalytic infrared radiation panel and investigate powder coating curing under various radiant heating conditions. The coating quality was examined using five tests. The measured data obtained from these experiments were used to verify the model's reliability.

2.2.1. Catalytic Infrared Radiation Panel Characteristics Test

The radiant panel's performance affected the powder coating's curing quality. The radiant panel's surface temperature and surface radiation intensity were used to quantify its performance. In this study, the surface temperature of the radiant panel was tested with different gas flow rates and the surface radiation intensity was tested with different wavelengths.

2.2.2. Fourier-Transform Infrared Spectroscopy of the Powder Coatings

Fourier-transform infrared (FT-IR) spectroscopy (Thermo-Nicolet, Waltham, MA, USA) was employed to investigate the chemical structure of the powder coatings. The potassium bromide tablet method was used for testing, and the test range was set to 500~4000 cm^{-1}.

2.2.3. Curing Methods and Test Conditions

A sample plate sprayed with a powder coating was placed on the internal platform underneath the radiant panel, and the coating temperature was increased to 180 °C, 190 °C, 200 °C, 210 °C, 220 °C, 230 °C, and 240 °C by controlling the gas flow into the radiation

panel. The sample plate was held at these seven temperatures with 1 min intervals for 1 to 5 min, respectively. After heating, the sample plate was removed and cooled to ambient temperature.

The curing process potentially affects the mechanical properties of cured samples, such as the hardness, flexibility, impact resistance, appearance of the film surface, and chemical resistance [4,30]. Therefore, five mechanical properties of these cured samples were tested: adhesion, impact resistance, gloss, pencil hardness, and coating color. The test equipment and processes are shown in Figure 5.

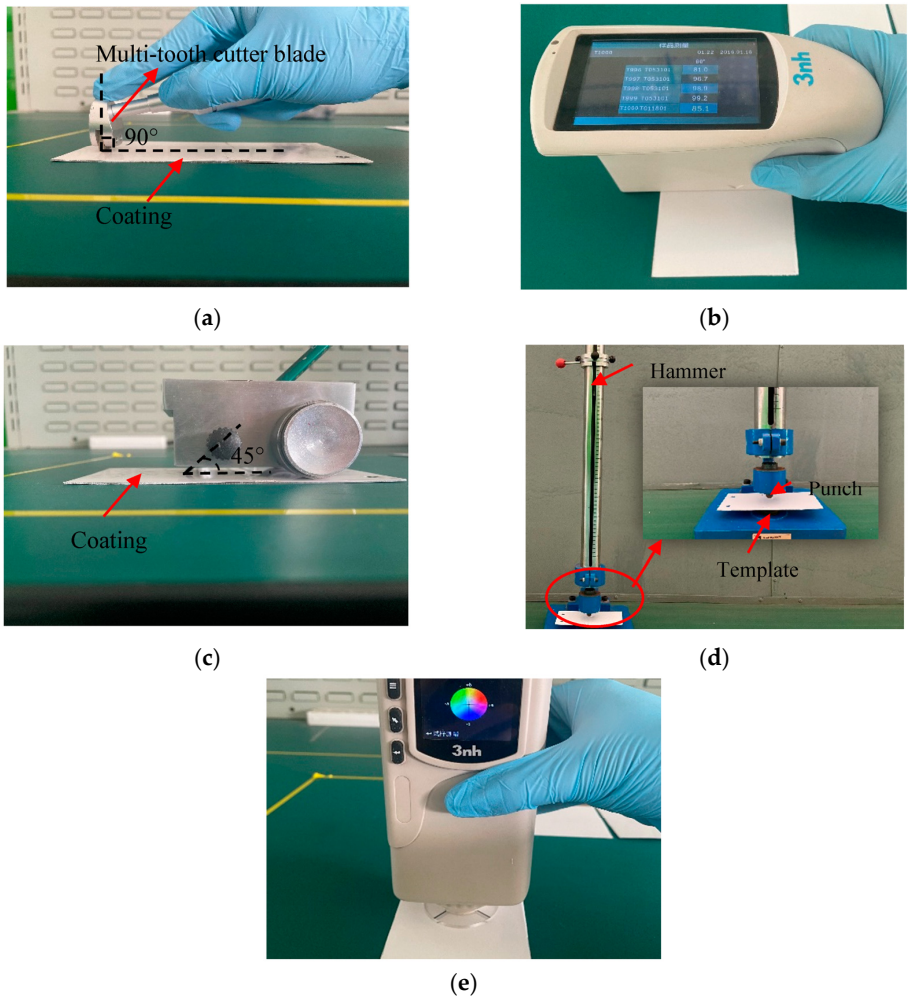


Figure 5. Test equipment and processes: (**a**) adhesion test, (**b**) gloss test, (**c**) hardness test, (**d**) film impact resistance test, and (**e**) color test.

The test methods were as follows:

Adhesion: This test was conducted according to ASTM Test Method D3359, Method B using a multi-toothed blade (QFH-A, Dongguan Huanguo Precision Instrument Co., Ltd., Dongguan, China) suitable for standard adhesion tests. Specific method: Firstly, the cured coating template was fixed, and the multi-toothed cutter blade was set perpendicular to the template and drew a scratch. Then, the template was evenly covered with transparent tape before it was removed to observe the scratching off, using the observer's judgment to determine the size of the adhesion area;

Gloss: This test was performed with a gloss meter measuring instrument (HG-60, Shenzhen Threenh Technology Co., Ltd., Shenzhen, China). Specific method: A calibrated gloss meter was placed on the coating so that no light entered, and the beam of the internal light source of the instrument was at an angle of 60° from the normal line of the tested coating surface.

Then, the instrument was initiated and it read the gloss value of the coating. This test was conducted according to ASTM Test Method D523;

Hardness: The pencil thickness meter (Shanghai Gaozhi Precision Instrument Co., Ltd., Shanghai, China) was used to test the hardness of the cured films. This test was conducted according to ASTM Test Method D3363. Specific method: After curing, a pencil with the same hardness was used for three scratch tests to observe the damage to the template. The hardness of the hardest pencil that did not leave scratches larger than 3 mm on the coating was used as an indication of the hardness of the coating;

Impact resistance: In this test, a paint film impactor (QCJ-50/100, Tianjin Expo Weiye Hua Glass Instrument Co., Ltd., Tianjin, China) was used to test the hardness of the cured films. This test was conducted according to ISO 6272-2:2002. Specific method: The prepared coating was placed on the anvil at the lower part of the instrument. The hammer was lifted to 50 cm and allowed to fall freely, impacting the template. The damage to the coating surface was recorded;

Color: The colors of the coating surfaces were measured using a universal colorimeter (NR10QC, Shenzhen Threenh Technology Co., Ltd., Shenzhen, China). Specific method: A calibrated universal colorimeter was placed on the surface of the coating and activated to take readings.

Errors were mainly introduced in the operation for the testing of the mechanical properties (adhesion, hardness, and impact resistance) and due to the accuracy of the instruments for the gloss and color testing. Following the mechanical property tests performed with epoxy powder coatings in the study by Jingwen Zhang et al. [8], all tests were carried out three times to check the repeatability.

2.3. Experimental Results and Discussion

2.3.1. Characteristics of the Catalytic Infrared Radiation Panel

The surface temperature of the radiant panel was mainly controlled by the intake gas volume, and the relationship between the surface temperature and gas flow is shown in Figure 6a. The surface temperature of the radiant panel reached a maximum of 475 °C when the intake gas flow was 0.3 m^3/h. When the gas flow was increased above 0.3 m^3/h, the surface temperature decreased due to the excessive gas flow. At excessively high flow rates, the gas did not have enough time to react with and diffuse into the environment around the surface of the radiant panel. Moreover, the oxygen on the surface of the radiant panel was swept away, resulting in insufficient oxygen and an incomplete gas reaction.

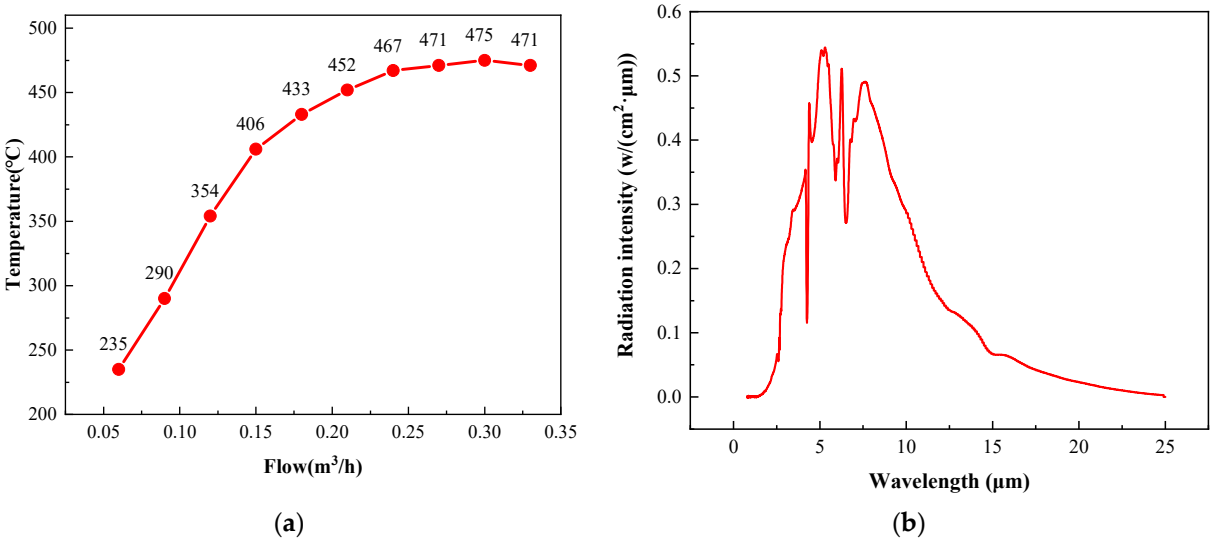


Figure 6. (**a**) Relationship between the surface temperature of the radiant panel and the gas intake. (**b**) The catalytic infrared radiation intensity of the radiant panel.

Infrared radiation (IR) can be divided into three categories according to the wavelength: near-infrared (NIR), mid-infrared (MIR), and far-infrared (FIR) radiation. A wavelength range of 0.75–2 μm is generally defined as NIR, 2–4 μm as MIR, and 4–1000 μm as FIR [31]. The catalytic infrared radiation intensity curve obtained in this study is shown in Figure 6b. The measured wavelengths were in the range of 2–25 μm. Thus, this radiation was both MIR and FIR.

2.3.2. FT-IR Analysis

FT-IR spectroscopy measures a sample's characteristic vibrational absorption bands to determine its chemical structure [32]. The infrared spectra of the powder coatings are shown in Figure 7. The absorption peaks of the functional groups were in the wavenumber range of 4000–500 cm^{-1} (with a corresponding wavelength range of 2.5–20 μm). The most intense absorption peaks were located in the wavenumber range of 2000–500 cm^{-1} (with a corresponding wavelength range of 5–20 μm). Therefore, the infrared radiation panel's infrared radiation range covered the absorption wavelengths of the powder coating's functional groups.

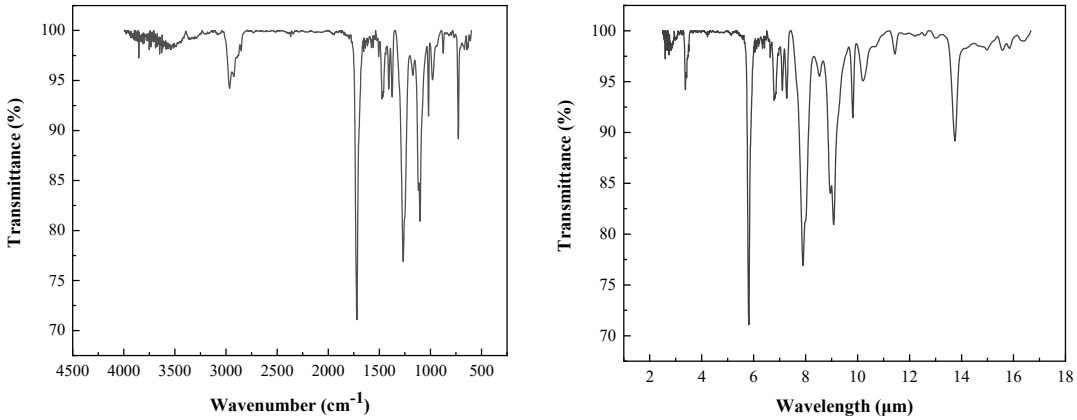


Figure 7. The infrared spectra of the polyester-based/TGIC powder coating: (**a**) variation with wavenumber and (**b**) variation with wavelength.

Moreover, most absorption peaks were located in the range of 5–10 μm, matching the most intense infrared radiation wavelengths emitted by the radiation panel. Under the radiant panel, the functional groups of the coating absorbed infrared radiation energy and converted it into vibrational energy. At the same time, intermolecular energy transfer and whole-molecule resonance led to a crosslinking reaction and accelerated the curing of the powder coating.

2.3.3. Catalytic Infrared Heating Performance

During infrared radiation heating, the temperature difference between the top of the substrate (coating) and the bottom of the substrate is one factor determining the curing quality. If the temperature difference between the top and bottom is too great, there is a large temperature gradient inside the substrate, and the coating and the substrate may have poor adhesion.

As shown in Figure 8, within 1 min of the beginning of heating, the top and bottom of the substrate had a significant slope and the temperature rose rapidly, indicating that the catalytic infrared radiation could heat the coating and the substrate rapidly. In addition, the maximum temperature difference between the top and bottom of the substrate did not exceed 7 °C during the curing process, which indicated that the temperatures of the substrate and the coating remained almost consistent during the curing process, which was conducive to the bonding of the coating and the substrate.

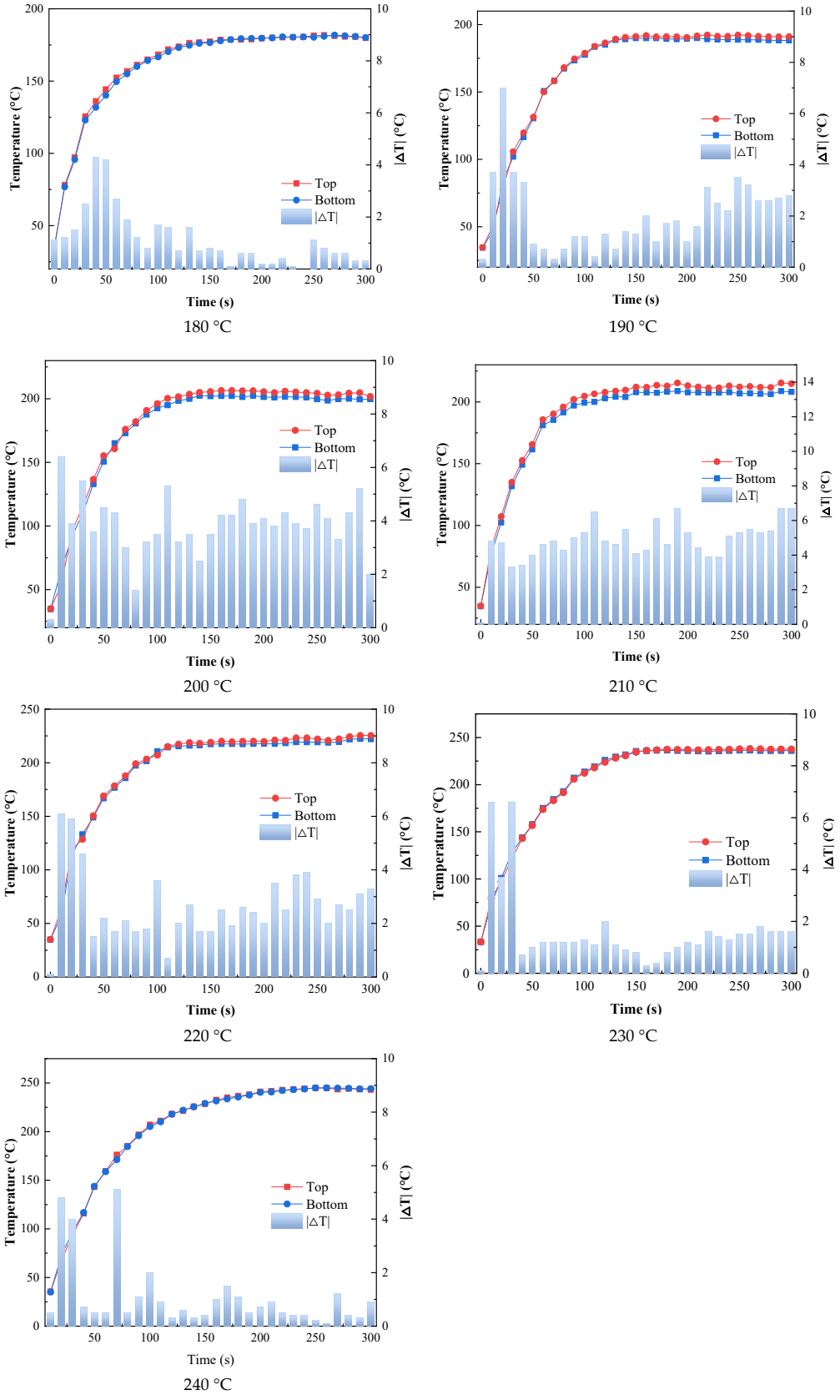


Figure 8. Variation in coating temperature and substrate bottom surface temperature with time.

2.3.4. Curing Tests

Adhesion

The adhesion results for the cured products after curing with catalytic infrared radiation are shown in Figure 9. A rating higher than 4B is generally considered a qualified product [14], and the rating standards are shown in Table 4. With increasing curing temperature and curing time, the adhesion level of the coating increased. This was due to the enhanced degree of bonding between the coating and the substrate. When the curing temperature was 200 °C and the curing time was 5 min, an adhesion rating of 5B was obtained, meeting engineering requirements. With a curing temperature of 230 °C or 240 °C, a curing time of only 2 min was required to achieve an adhesion rating of 5B. Jong Won Choi et al. [14] used NIR radiation to cure a solvent-blended acrylic resin with an amine crosslinker coating, which did not meet the 4B standard. However, they combined an NIR curing system with a convective oven to obtain a coating that met this standard. The maximum allowable temperature for solvent-based coatings is generally low, and the high-power density of an infrared heater may induce thermal stress between the substrate and the coating, resulting in defects, such as local cracks and film deletion.

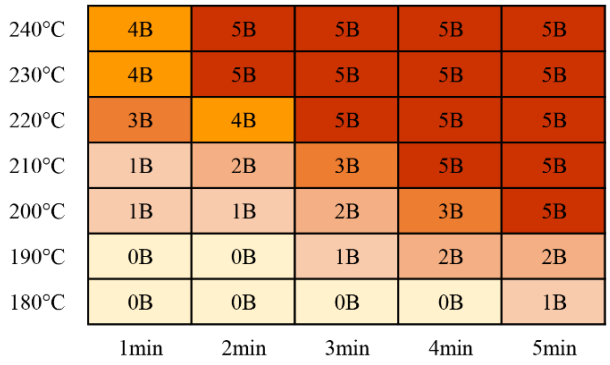


Figure 9. Coating adhesion test results.

Table 4. Classification chart for paint adhesion tests [14].

Grade	Area Removed	Cross-Cut Area of Six Parallel Lines
5B	None	
4B	Less than 5%	
3B	5–15%	
2B	15–35%	
1B	35–65%	
0B	Greater than 65%	

In contrast, powder coatings' maximum allowable temperature is generally high, and they do not have a solvent component. Therefore, powder coatings are more suitable for infrared curing. However, excessively high coating temperatures inevitably change other physical properties, such as color and gloss.

Gloss

Gloss is an optical property that indicates how the surface reflects light in a specular (mirror-like) direction [33]. The gloss of a colored powder system depends on the degree of dispersion and particle size distribution of the pigments, and gloss has little effect on the infrared absorptivity of coatings [34]. However, gloss affects the appearance of coatings. Therefore, the average gloss values for ten points on each sample were measured for analysis. The coating gloss decreased with increasing temperature for each curing time, as shown in Figure 10. The coating gloss significantly declined at curing temperatures higher than 220 °C. As shown in Figure 11, the curing time slightly affected the gloss at temperatures below 210 °C. The gloss values achieved at these low curing temperatures were within the gloss range required for the coatings (90 ± 5). When the temperature exceeded 210 °C, the gloss sharply decreased with increasing curing time. When the curing time was 5 min and the curing temperature was 240 °C, the average gloss of the coatings decreased to below 85. This demonstrated the importance of controlling the temperature of the coating during curing.

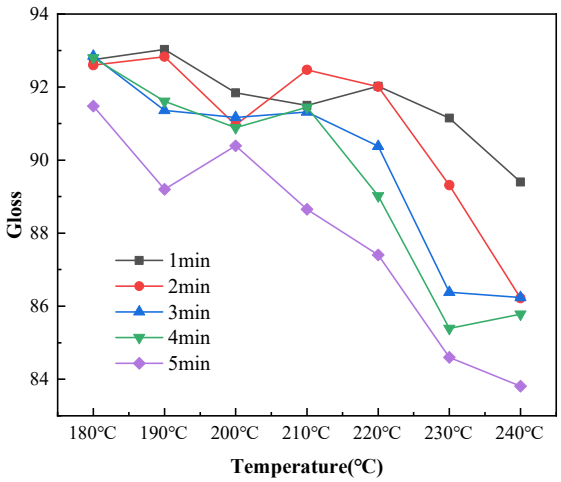


Figure 10. Changes in the coating gloss with curing temperature after different curing times.

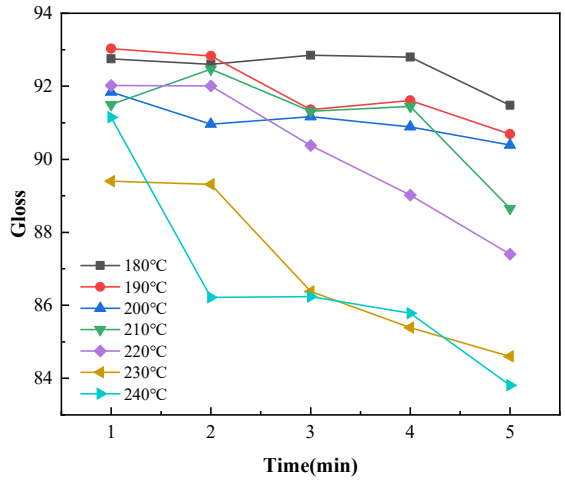


Figure 11. Changes in the coating gloss with curing time with different curing temperatures.

Hardness

Coating hardness increased with increasing curing time and temperature, as shown in Figure 12. Most of the tested curing parameters resulted in coating hardness ratings that were better than H (meeting the minimum requirement for these coatings). It was determined during the testing that thinner coatings exhibited higher pencil hardness ratings than thicker coatings with the same curing parameters. This was related to the physical properties of the coatings and the substrates.

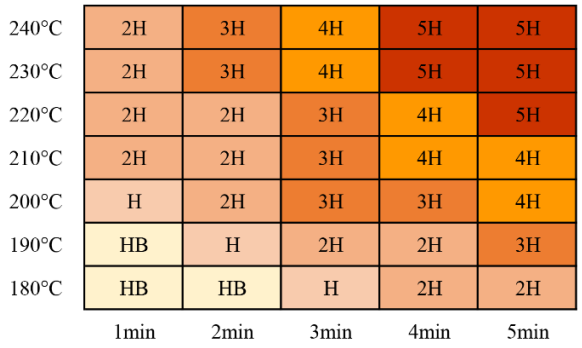


Figure 12. Coated pencil hardness test results for the coatings.

Impact Resistance

Impact resistance, also known as impact strength, refers to the ability of a film on a substrate to rapidly deform under a heavy hammer impact without cracking or peeling away from the substrate. This test was performed to evaluate the flexibility of the coatings and their adhesion to the substrate. In this test, the impact height was 50 cm. As shown in Figure 13, the impact test did not generate cracks when the coating was cured at 200 °C for 5 min. Thus, the shortest curing time required for the coating at 200 °C was 5 min. Similarly, at curing temperatures of 210 °C, 220 °C, 230 °C, and 240 °C, the shortest curing times were 4 min, 3 min, 2 min, and 2 min, respectively.

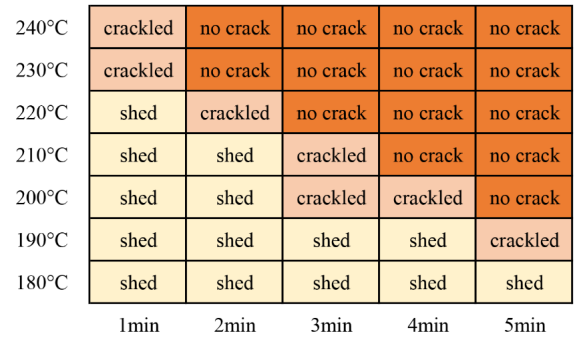


Figure 13. Impact resistance test results for the coatings.

Color

The laboratory color model developed by the International Commission on Illumination (CIE) can be used to describe human visual effects digitally. This lab color model consists of three elements: brightness (L*) and the color channels a* and b*. The term L* describes brightness and has potential values ranging from 0 (black) to 100 (white). The a* coordinates represent the redness and greenness of a sample. The b* coordinates represent the yellowness and blueness of a sample [35]. The coordinate ranges of a* and b* are approximately [−100, 100]. In this model, it was determined that the color of the tested coatings did not significantly change when varying the curing time at a fixed curing temperature. Therefore, the average values of L*, a*, and b* measured at different temperatures were assumed to be representative test values for those temperatures. Figure 14 shows that,

as the temperature increased, the a* value of the coating gradually decreased—that is, the "red" value decreased. The b* and L* values initially increased with increasing temperature. However, these values decreased when the curing temperature exceeded 230 °C. In particular, the value of L* sharply decreased at excessively high curing temperatures. These results demonstrated that high temperatures had a strong effect on coating brightness.

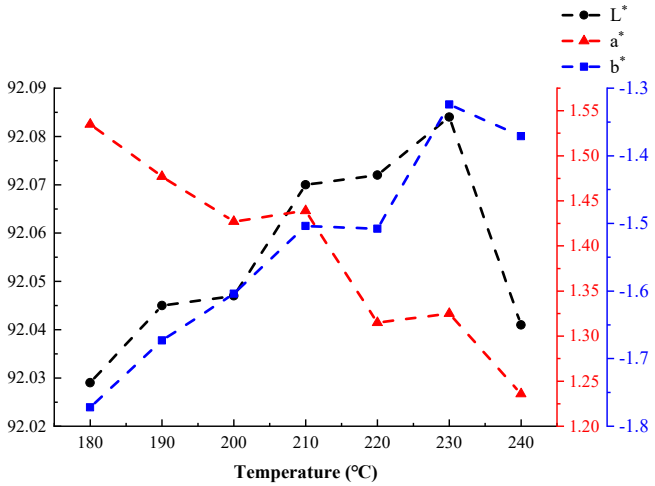


Figure 14. The effects of temperature on the coatings' CIE laboratory color model values.

Summary

The tests described in this section showed that the curing time decreased with increasing curing temperature because high temperatures increased the crosslinking of the powder molecules. The mechanical property and appearance requirements could be satisfied when a curing temperature of 200 °C was maintained for 5 min. This reduced the time by half compared to the hot-air curing conditions provided by the coating manufacturer (Table 3), which have to be maintained at 200 °C for 10 min. All of the test results met the requirements when the curing parameters were 220 °C for 3 min and 230 °C for 2 min. Considering energy consumption, efficiency, and coating quality, 220 °C for 3 min and 230 °C for 2 min were considered the best curing parameters. The optimal curing parameters were consistent with the values from the adhesion and impact tests, and the results of the hardness test at 210 °C and 1 min met the requirements. Gloss requirements were satisfied at 180 °C and 1 min. The results for the color tests met the requirements, except for a sharp drop in L* values and a darkening of the coating at 240 °C. This was due to a sufficient temperature and time for the crosslinking reaction of the molecules inside the coating being used, ensuring better adhesion between the coating and substrate. The gloss and color were mainly related to the color filler in the coating composition, and the appearance of the coating deteriorated when the polyester resin, titanium dioxide, and other components in the coating aged and darkened after spending too much time in the high-temperature range. Consequently, a lower curing temperature was considered to be better for gloss and color.

To further evaluate whether the curing parameters obtained in this study were efficient, we compared the curing parameters required for powder coatings using catalytic infrared curing with those required by other curing methods described in the literature. As shown in Table 5, the infrared heating method improves efficiency compared to the traditional hot-air heating method. The optimal curing parameters obtained in this study could reduce the time required by 80–90% compared to the hot-air curing parameters provided by the coating manufacturer.

Table 5. Comparison of curing parameters with those obtained from the literature.

Sr.	Coating Type	Curing Method	Curing Parameter	Ref.
1	Epoxy resin-modified PVC powder coating	Hot-air oven	180 °C for 10 min	[6]
2	Polyester-based powder coating	Hot-air oven	180 °C for 15 min	[7]
3	Epoxy powder coating	Hot-air oven	210 °C for 10 min	[8]
4	Polyester-based powder coating	Hot-air oven	150 °C for 15 min	[9]
5	Polyester/epoxy/acrylic resin powder coating	Hot-air oven	160 °C for 10 min	[36]
6	Solvent-blended acrylic resin with an amine crosslinker coating	NIR system	200 °C/5–15 min	[14]
7	Polyester-based powder coating	Catalytic infrared	220 °C for 3 min 230 °C for 2 min	This study

The coating temperature was not maintained at a constant value when it was controlled; it fluctuated up and down. Moreover, there was an unavoidable error in the thermocouple. In addition, there were operational and instrumental errors in the subsequent coating test. Therefore, 220 ± 5 °C for 3 min and 230 ± 5 °C for 2 min can be considered as the optimal curing parameters for the production process.

3. Numerical Simulations

The experimental test results reported in Section 2 demonstrated that the curing temperature and curing time had apparent influences on the mechanical properties of the coatings. A short curing time and low temperature led to lower adhesion between the finished coating and the substrate. An excessively long curing time and excessively high curing temperature negatively affected the appearance of the coating (e.g., gloss, color). Therefore, a model that can predict the effect of temperature changes is required for actual production processes to allow for better product quality control.

3.1. Geometric Model

The geometric model consisted of the powder coating and metal substrate, as shown in Figure 15. The dimensions of the coating and substrate are shown in Table 6, and the thermophysical properties of the coating and substrate are reported in Table 7. The paint's thermophysical properties (specific heat capacity, density, ε) were obtained from the literature [13]. Suzhou Catalytic Green Energy Co., Ltd. provided the thermophysical properties of the substrate.

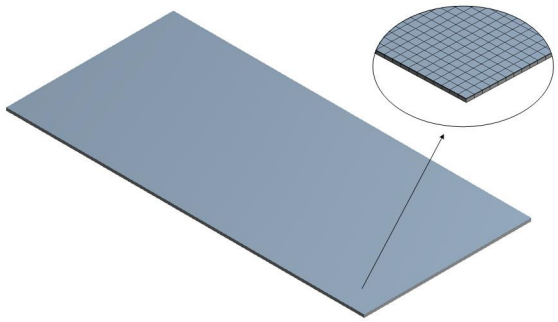


Figure 15. Geometric model consisted of the powder coating and metal substrate.

Table 6. Dimensions of the coating and substrate.

Material	Length (mm)	Width (mm)	Thickness (mm)
Coating	150	70	0.1
Substrate	150	70	1

Table 7. Thermophysical properties of the coating and substrate.

Material	Thermal Conductivity W/m·°C	Specific Heat Capacity J/kg·°C	Density kg/m^3	ε
Coating	0.1	1500	1590	0.91
Substrate	44.5	460	8237	0.92

3.2. Heat Transfer Model

Radiative heat transfer occurred between the radiant panel and the coating surfaces. The coatings were very thin, and the thickness was low compared to the area of the coatings. Moreover, the radiative effect of the air on the coatings was weak. Therefore, the following assumptions and simplifications concerning the heat transfer process were made:

1. The film was isotropic and homogeneous, the coating temperature was uniform and consistent before curing, and the film thickness did not change during curing;
2. The density, thermal conductivity, specific heat capacity, and other physical properties of the coating and substrate were constant and did not change with temperature;
3. The thickness of the coating was set to e_p, and heat transfer only occurred in the Z direction;
4. Assuming that the heat transfer process was uniform, the heat transfer model in the substrate was simplified as one-dimensional heat transfer along the Z direction;
5. The radiative effect of air was not considered.

Due to the complexity of radiative heat transfer and the convenience of computational models for establishing stable heat transfer simulations, the model was simplified with the following assumptions:

1. Infrared rays have a specific penetration capability, and objects can be simultaneously heated within this penetration distance. Thus, the infrared heating rate of the coating was higher than that of hot-air heating. The thickness of the coating (100 μm) was within this infrared penetration zone. Therefore, it was assumed that the temperature at every point in the coating simultaneously increased. Based on this analysis, the heat transfer process was simplified by equating the infrared radiation heating of the coating with the heating of the coating via an internal heat source;
2. The coating was very thin, so it was assumed that no attenuation of infrared radiation occurred along the thickness direction. Therefore, the intensity of the equivalent internal heat source within the coating was equal across all points in the coating.

Figure 16 shows the relevant heat transfer equations for the powder coating and the metal substrate. Due to the low coating thickness, the metal substrate was relatively thin and had good thermal conductivity. The coating was measured multiple times with a thermocouple during the experimental test process. The heat balance of the powder coating and metal substrate system is shown below [13,29]:

$$\frac{dT}{dt}\left(C_{p_p}\rho_p e_p + C_{p_s}\rho_s e_s\right) = \overline{Q}_{abs} - \overline{Q}_{emitted} - \overline{Q}_{convection} - \overline{Q}_{reaction} \quad (1)$$

$$\overline{Q}_{abs} A p = \eta_{tot} Q_{chem} \quad (2)$$

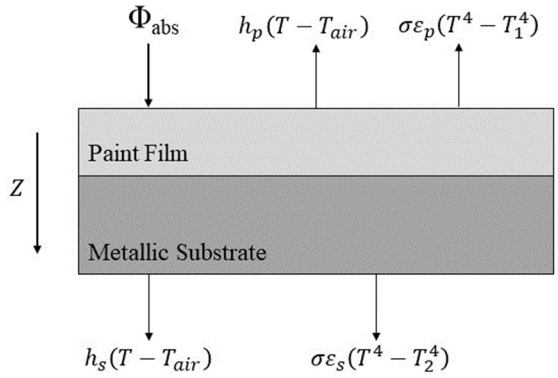


Figure 16. Heat transfer diagram for coating and substrate system (adapted from L. Véchot et al. [13]).

The heat released by the curing chemical reaction was negligible compared to the other heat flux values. Thus, it was ignored in the calculation [13]. The heat balance equation for the powder coating and metal substrate system was simplified as Equation (3):

$$\frac{dT}{dt}\left(C_{p_p}\rho_p e_p + C_{p_s}\rho_s e_s\right) = \overline{Q}_{abs} - \sigma\left[\varepsilon_s\left(Ts^4 - T_\infty^4\right) + \varepsilon_p\left(Tp^4 - T_\infty^4\right)\right] - \left[h_s(Ts - T\infty) + h_p(Tp - T\infty)\right] \quad (3)$$

The value of η_{tot} depends on the thermal efficiency of the radiation panel (η_R), as well as the thermal efficiency of the heat transfer from the radiation panel to the powder coating (η_{ht}) [37]. This relationship is shown in Equation (4). The radiation panel thermal efficiency was used to quantify the efficiency of the conversion of the chemical energy of the gas into radiation energy, as shown in Equation (5):

$$\eta_{\text{tot}} = \eta_R \eta_{ht} \quad (4)$$

$$\eta_R = \frac{Q_R}{Q_{chem}} \quad (5)$$

The radiation heat transfer efficiency was related to the heat energy Q_{abs} absorbed by the powder coating and the radiation energy Q_R of the radiation panel, in accordance with Equation (6):

$$\eta_{ht} = \frac{Q_{abs}}{Q_R} \quad (6)$$

The radiation panel area was much larger than the sample coating area, and the value of Q_{abs} was calculated according to Equation (7):

$$dQ_{abs} = \eta_{ht}\frac{E_R}{\pi}A_R dw \quad (7)$$

$$E_R = \frac{Q_R}{A_R} \quad (8)$$

$$dw = \frac{dA_p}{l^2} \quad (9)$$

Due to the characteristics of the infrared heating coating and the simplifications of this model, Q_{abs} was converted into an equivalent internal heat source Q_p using Equation (10):

$$Q_p = \frac{Q_{abs}}{V_p} = \frac{Q_{abs}}{A_p e_p} \quad (10)$$

Inserting Equations (4)–(9) into Equation (10) resulted in a linear relationship, as demonstrated by Equation (11):

$$Q_p = \frac{\eta_{tot} q_h}{\pi e_p l^2} q_V \quad (11)$$

If $Cg = \frac{\eta_{tot} q_h}{\pi e_p l^2}$, then:

$$Q_p = Cgq_V \quad (12)$$

3.3. Boundary Conditions

The coating and substrate temperatures were even and constant before the coatings were heated. An infrared thermometer was used to measure the initial temperature, which was 30 °C. The initial flow rate of the infrared radiant plate was 0.2 m^3/h, and the corresponding internal heat source value was 8.5 W/m^3. The ambient temperature was 80 °C (in the experimental testing, the actual temperature fluctuated around 80 °C by less than 5%). The values of h_p and h_s were 4.5 $W/m^2 \cdot °C$ and 9 $W/m^2 \cdot °C$, respectively [29]. The surface around the coating and substrate was simulated as an insulated boundary (the coating and substrate only exchanged heat with the surrounding air and did not heat the surface).

3.4. Numerical Method and Model Validation

3.4.1. Numerical Method

The finite element analysis software ANSYS Workbench 18.2 was used for the numerical simulation. The flow rate was set to 0.2 m^3/h (with a corresponding internal heat source value of 8.5×10^7 W/m^3), and the thickness of the substrate was 1 mm. With a time step of 1 s, grid sizes of 21,120, 28,080, and 32,480 were used for the simulation. The changes in the coating temperature with time for each group of grids are shown in Figure 17. The results of the 32,480 grid simulation differed from those of the 21,120 grid simulation by a maximum of 3.31 °C. To ensure the accuracy of the numerical simulation, the 32,480 grid size was used for subsequent simulations.

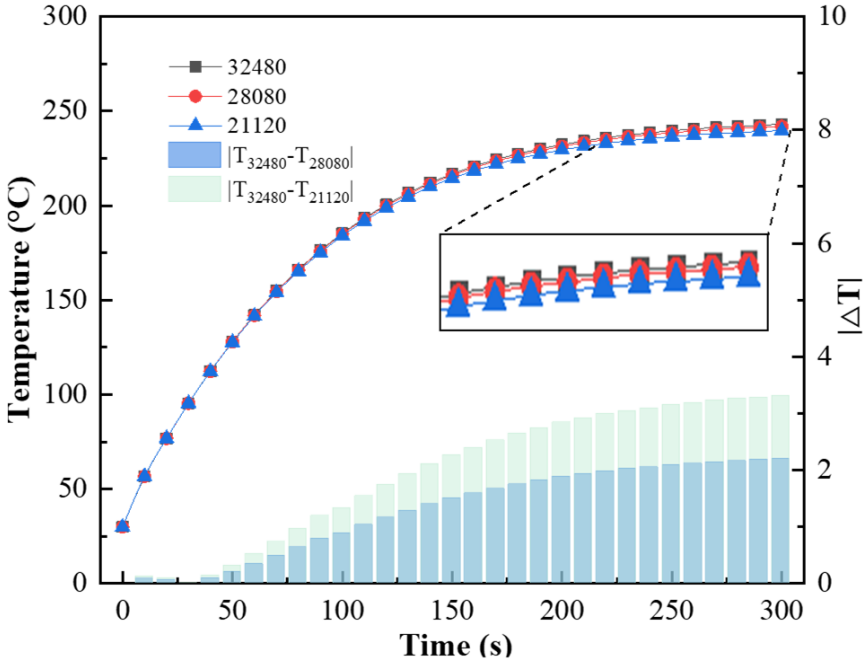


Figure 17. Coating temperature versus time with different grid sizes.

The changes in the coating temperature with three time steps (0.1 s, 1 s, and 10 s) are shown in Figure 18. During the coating heating process, the simulated coating temperature was lower when the time step was 10 s. Considering the time and accuracy of the simulation, 1 s was selected as the time step for subsequent simulations.

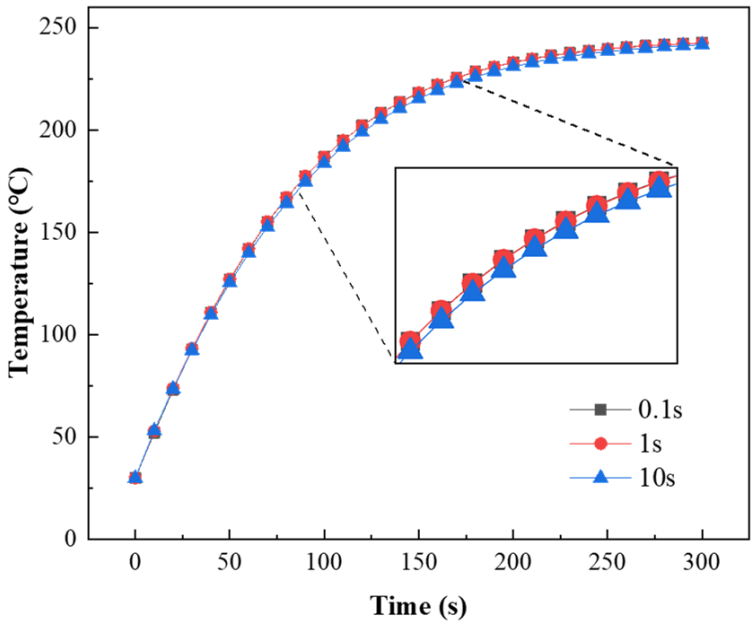


Figure 18. Coating temperature versus time with different time steps.

3.4.2. Model Validation

The total efficiency (η_{tot}) of powder coating curing with a gas infrared heater is between 25% and 30% [37]. However, the total efficiency of powder coating curing with catalytic infrared heating equipment is unknown. Experimental data with a curing temperature of 240 °C were used to determine the total efficiency value. The model was then validated using curing temperatures of 230 °C and 220 °C.

As shown in Figure 19, the simulation results closely matched the experimental results when η_{tot} was 0.4. The relative errors are shown in Table 8, and the maximum relative error was 7.6% at 1 min.

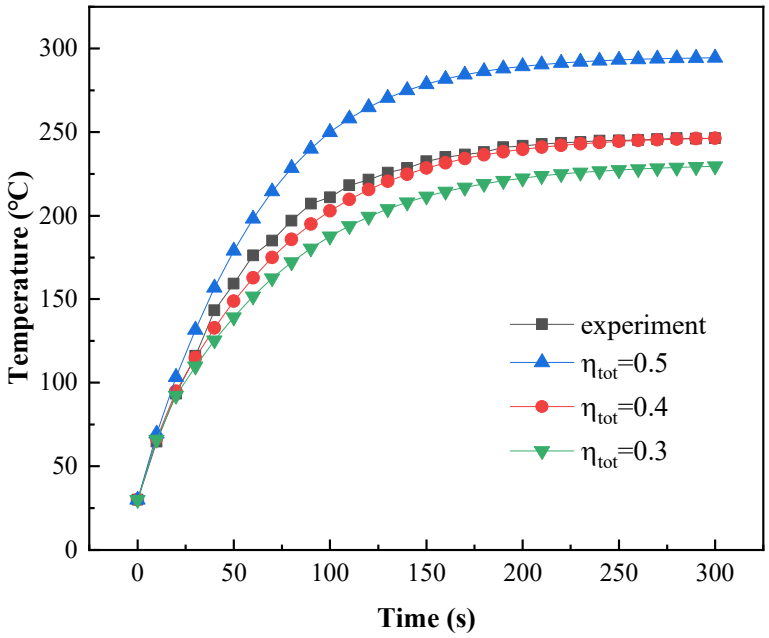


Figure 19. Comparison of measured and simulated coating temperatures.

Table 8. Relative errors for measured and simulated coating temperatures (η_{tot} = 0.4).

Time (s)	40	50	60	70	80	90
Experimental data (°C)	143.2	159.3	176.2	185.1	196.9	207.1
Simulated data (°C)	132.85	148.73	162.73	175	185.68	194.93
Relative error (%)	7.23%	6.64%	7.64%	5.46%	5.70%	5.88%
Time (s)	100	110	120	130	140	150
Experimental data (°C)	211	218.1	221.4	225.7	228.5	232.5
Simulated data (°C)	202.91	209.75	215.61	220.61	224.85	228.46
Relative error (%)	3.83%	3.83%	2.62%	2.26%	1.60%	1.74%

The model's accuracy was further verified using curing temperatures of 220 °C and 230 °C by changing the gas intake of the radiant panel. During the experimental process, the maximum gas flow rate of 0.20 m^3/h was used for the coating in the initial heating stage to ensure that it was rapidly heated. The gas flow was reduced when the coating reached the curing temperature. When the coating was heated for 125 s, the gas flow was decreased to 0.16 m^3/h. This maintained the curing temperature at 220 °C. When the coating was heated for 157 s, the gas flow was decreased to 0.18 m^3/h. This maintained the curing temperature at 230 °C. After adjusting the gas flow meter, the gas flow required approximately 30 s to stabilize. Therefore, when the simulated curing temperature was 220 °C, the initial internal heat source value was 8.5 W/m^3, and at 156 s, the internal heat source value was adjusted to 6.8 W/m3. When the simulated curing temperature was 230 °C, the initial internal heat source value was 8.5 W/m^3, and at 188 s, the internal heat source value was adjusted to 7.65 W/m^3.

The simulation results are shown in Figure 20. The simulated temperature values were lower than the measured temperature values during the entire heating process. This was because the radiation intensity of the radiation panel was delayed after the gas flow to the radiation panel was reduced during the heating process. The maximum differences between the simulation and experimental data were 8.7% at 230 °C and 9.6% at 220 °C. Therefore, this model can accurately predict changes in coating temperatures in engineering applications.

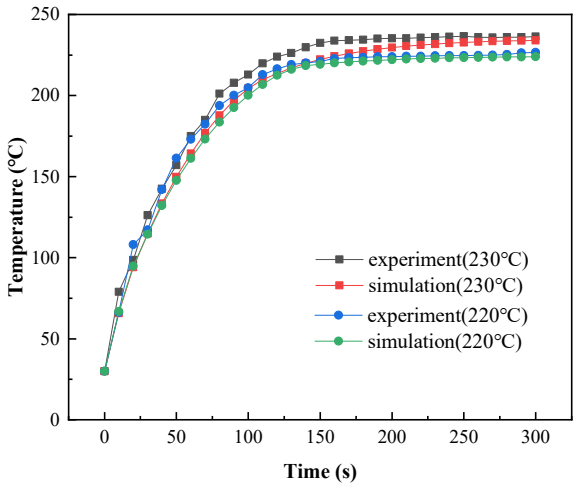


Figure 20. Comparison of experimental and simulated temperatures during the curing process.

3.5. Simulation Results and Discussion

Temperature nephograms obtained at curing temperatures of 220 °C and 230 °C are shown in Figure 21. The convective heat transfer coefficient of the coating surface was low, and the heat loss from this surface was also low. Therefore, in the initial phase of heating, the upper layer of the coating had a higher temperature. The coating surface was heated for 155 s to achieve a curing temperature of 220 °C. This curing temperature was maintained for 3 min. Then, the coating surface was heated for 187 s to achieve a curing

temperature of 230 °C. This curing temperature was maintained for 2 min. During this heating process, the temperature distribution of the coating became more uniform, with the highest temperature located in the middle of the coating. The internal temperature of the substrate was almost constant throughout the entire heating process.

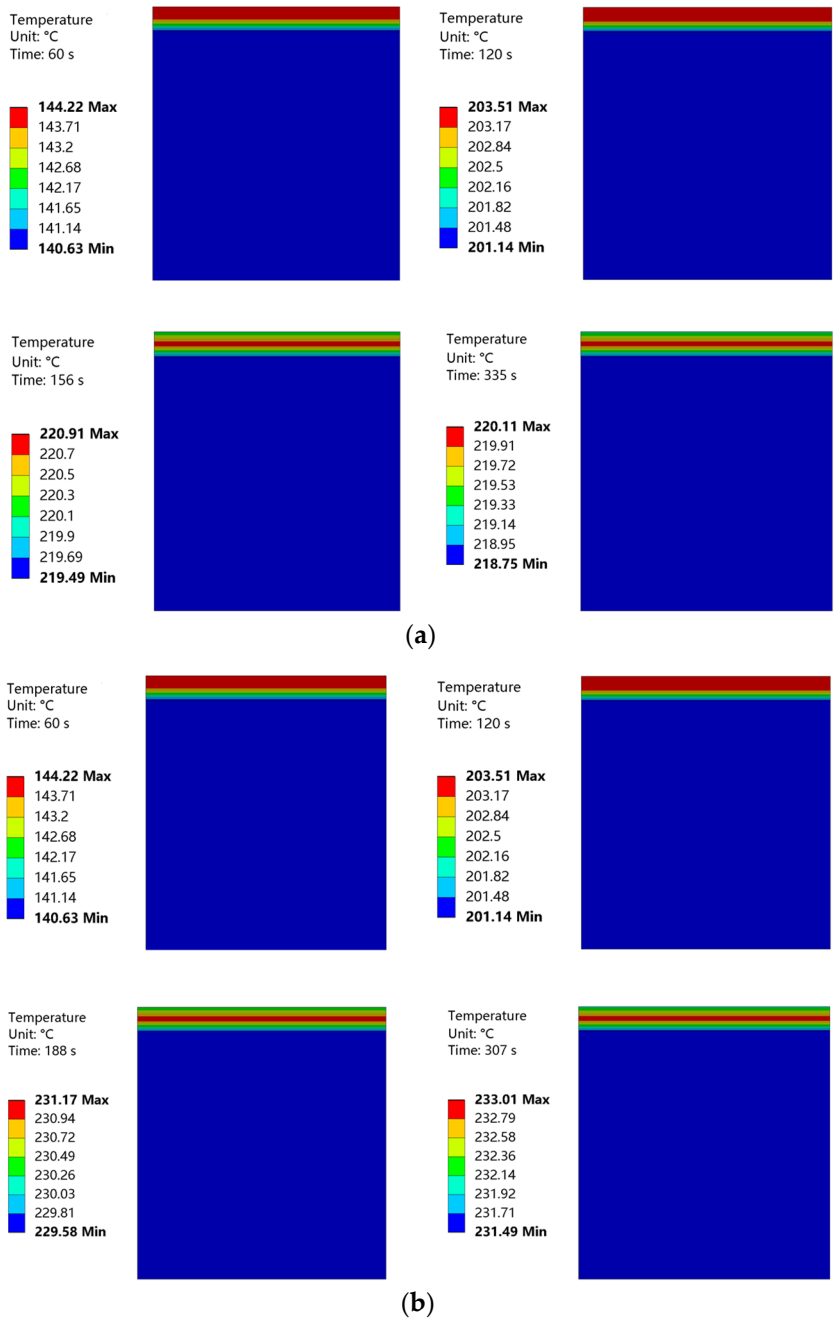


Figure 21. (**a**) Temperature nephogram of coating and substrate at a curing temperature of 220 °C. (**b**) Temperature nephogram of coating and substrate at a curing temperature of 230 °C.

To further analyze the heat transfer during the curing process and to provide a reference for production, numerical simulations were used to predict the coating temperature with different substrate thicknesses. The effects of metal substrate thicknesses ranging from 1 mm to 10 mm on the coating temperature were calculated using a gas inlet flow of 0.2 m^3/h. As shown in Figure 22, the rate at which the coatings were heated decreased with increasing substrate thickness. Figure 23 shows the predicted times required for the coating temperature to reach 220 °C or 230 °C with different substrate thicknesses. When the

substrate thickness was 1 mm, the coating required 2.58 min to reach 220 °C and 3.12 min to reach 230 °C. The minimum times required to cure the coatings with this catalytic infrared heating equipment were 5.58 min and 5.12 min for curing temperatures of 220 °C and 230 °C, respectively. Moreover, a shorter total curing time was required with a curing temperature of 230 °C, resulting in energy savings. Therefore, it is recommended that a curing temperature of 230 °C should be used when the substrate thickness is 1 mm, and 220 °C should be used when the substrate thickness is ≥2 mm.

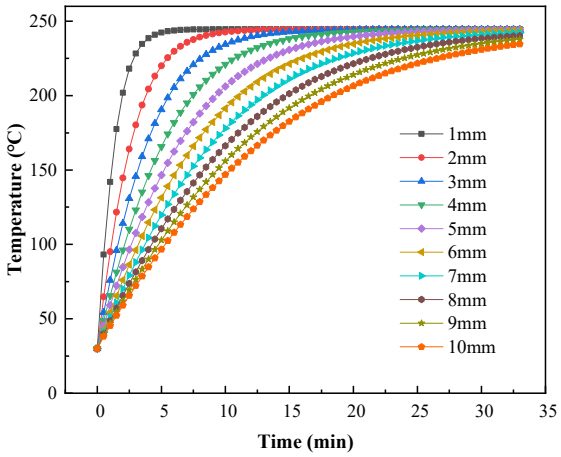


Figure 22. Predicted coating temperatures with varying substrate thickness.

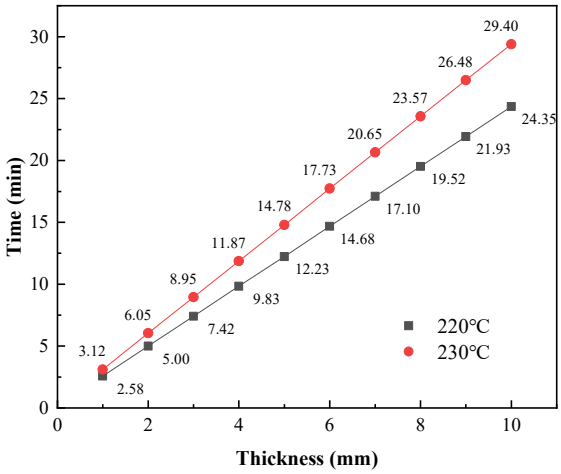


Figure 23. Heating times required for the coating temperature to reach 220 °C and 230 °C with different substrate thicknesses.

4. Conclusions

In this study, we designed a catalytic infrared curing system by combining catalytic infrared technology and coating curing equipment. The radiative characteristics of the catalytic infrared equipment were tested, and the applicability of this curing system for curing powder coatings was investigated. Finally, a one-dimensional heat transfer model was established. The following conclusions were obtained:

1. The maximum surface temperature of the radiation panel was 475 °C, and its infrared wavelength range was 2–25 μm. The infrared absorption wavelengths of most of the functional groups of the polyester/TGIC powder coatings were in this region. Thus, the coatings were quickly cured with catalytic infrared radiation;
2. The optimal curing parameters for this catalytic infrared curing process were 230 °C for 2 min and 220 °C for 3 min. The mechanical properties of the coatings became

stronger as the temperature and time increased. However, the gloss of the coatings appeared to decrease. When the temperature was too high, the color of the coatings became dark;

3. An internal heat source was introduced in the simulation model. This model could accurately predict the temperature change in the coating. The total efficiency η_{tot} was determined to be 0.4;
4. According to the numerical simulations, when the substrate thickness was 1 mm, the optimal coating curing temperature was 230 °C. For substrate thicknesses $\geq$ 2 mm, a coating curing temperature of 220 °C was more efficient.

This study showed that catalytic infrared radiation can be used to cure polyester-based coatings efficiently, and that the coatings can meet engineering quality requirements. Using the catalytic infrared optimal curing parameters determined in this study, the yield can be increased by four to nine times with the same production time compared to the hot-air curing parameters provided by the coating manufacturer. Compared to the curing parameters provided in the literature [7,9] for polyester-based coatings, the yield can be increased by 6.5 times with the same production time.

The simulation model reported in this work can be used to predict the shortest time required to cure coatings with different substrate thicknesses. This work is a significant reference for the design of production processes and catalytic infrared curing production lines. The catalytic infrared curing method is more suitable for application with high-temperature-resistant coatings, ensuring efficiency and savings in energy. Future research should focus on controlling the wavelength of catalytic infrared radiation to ensure a good match between the radiation wavelength and the infrared absorption band of the coating when producing different types of coatings, thus further reducing energy consumption and increasing yield.

Author Contributions: Conceptualization, S.P.; Methodology, Y.Y.; Software, Y.Y.; Validation, Y.Y.; Formal analysis, Y.Y. and T.W. (Tongzhao Wang); Resources, L.L.; Writing—original draft, Y.Y.; Writing—review & editing, T.W. (Tongzhao Wang), L.X., Y.L., X.W. and T.W. (Tian Wang); Visualization, Y.Y.; Supervision, S.P. and L.X. All authors have read and agreed to the published version of the manuscript.

Funding: The research was funded by the 13th Five-Year National Science and Technology Major Project of China (grant nos 2016YFC0801706 and 2017YFC0702202) and the National Natural Science Foundation of China (grant no. 51578011).

Data Availability Statement: Not applicable.

Acknowledgments: The authors are grateful for the financial support from the Key Laboratory for Comprehensive Energy Saving of Cold Regions Architecture of the Ministry of Education. The authors are also grateful for the financial support from the International Science and Technology Cooperation Center in Hebei Province (no. 20594501D).

Conflicts of Interest: The authors declare no conflict of interest. The funders had no role in the design of the study; in the collection, analyses, or interpretation of data; in the writing of the manuscript; or in the decision to publish the results.

Abbreviations

The following abbreviations are used in this manuscript:

A_p Powder coating area, m^2
A_R Radiation panel area, m^2
Cg Conversion factor
C_{p_p} Specific heat capacity of the paint, J/kg·°C
C_{p_s} Specific heat capacity of the substrate, J/kg·°C

e_p	The thickness of the paint, mm
e_s	The thickness of the substrate, mm
E_R	Radiation force of the radiation panel, W/m^2
h_p	Convective heat transfer coefficient for the coating, W/m·°C
h_s	Convective heat transfer coefficient for the substrate, W/m·°C
l	Distance between the radiant panel and the coating, m
$\overline{Q}_{abs}$	Infrared radiation absorbed by the powder coating, W/m^2
$\overline{Q}_{convection}$	Convection heat flux between the system and air, W/m^2
$\overline{Q}_{emitted}$	Radiation heat flux between the system and environment, W/m^2
$\overline{Q}_{reaction}$	Heat released by the exothermic chemical reaction, W/m^2
Q_{abs}	Heat absorbed by the powder coating, W
Q_{chem}	The chemical energy of gas, W
Q_p	Internal heat source, W/m^3
Q_R	Radiation panel radiation energy, W
T_∞	Air temperature, °C
T_s, T_p	The temperatures of the upper and lower surfaces, °C
Greek symbols	
w	Solid angle, sr
ε	Emissivity
η	Efficiency
ρ	Volume mass, kg·m^{-3}
σ	Boltzmann constant, W·m^{-2}·K^{-4}
Subscripts	
Chem	Chemical
ht	Radiant heat transfer
p	Powder coating
R	Radiation
s	Metallic substrate
tot	Total

References

1. Biller, K.; The Powder Coating Research Group. New Advances in Powder Coating Technology. *Focus Powder Coat.* **2021**, *2021*, 4–5. [CrossRef]
2. Ayrilmis, N. A review on electrostatic powder coatings for the furniture industry. *Int. J. Adhes. Adhes.* **2022**, *113*, 103062. [CrossRef]
3. Czachor-Jadacka, D.; Pilch-Pitera, B. Progress in development of UV curable powder coatings. *Prog. Org. Coat.* **2021**, *158*, 106355. [CrossRef]
4. Misev, T.A.; van der Linde, R. Powder coatings technology: New developments at the turn of the century. *Prog. Org. Coat.* **1998**, *34*, 160–168. [CrossRef]
5. Ma, H.; Liu, Y.; Guo, J.; Chai, T.; Suming, J.; Zhou, Y.; Zhong, L.; Deng, J. Synthesis of a novel silica modified environmentally friendly waterborne polyurethane matting coating. *Prog. Org. Coat.* **2020**, *139*, 105441. [CrossRef]
6. Wang, C.; Han, Y.; Wang, W.; Liu, J.; Wang, N.; Hou, B. Polyvinyl chloride/epoxy double layer powder coating enhances coating adhesion and anticorrosion protection of substrate. *Prog. Org. Coat.* **2021**, *158*, 106335. [CrossRef]
7. Puig, M.; Cabedo, L.; Gracenea, J.J.; Jiménez-Morales, A.; Gámez-Pérez, J.; Suay, J.J. Adhesion enhancement of powder coatings on galvanised steel by addition of organo-modified silica particles. *Prog. Org. Coat.* **2014**, *77*, 1309–1315. [CrossRef]
8. Zhang, J.; Kong, G.; Li, S.; Le, Y.; Che, C.; Zhang, S.; Lai, D.; Liao, X. Graphene-reinforced epoxy powder coating to achieve high performance wear and corrosion resistance. *J. Mater. Res. Technol.* **2022**, *20*, 4148–4160. [CrossRef]
9. Jiang, R.; Zou, L.; Bi, H.; Zhang, Q. Research on the preparation of low temperature curing powder coatings. *J. Huangshan Univ.* **2021**, *23*, 50–53. (In Chinese)
10. Devisetti, S.K.; Burcham, L.J.; Macqueen, R.C. Dominant Factors of Gloss Control in Radiation Curable Coatings. 2008. Available online: https://www.radtech.org/proceedings/2008/papers/109.pdf (accessed on 18 October 2021).
11. Knischka, R.; Lehmann, U.; Stadler, U.; Mamak, M.; Benkhoff, J. Novel approaches in NIR curing technology. *Prog. Org. Coat.* **2009**, *64*, 171–174. [CrossRef]
12. Kyung, J.P.; Dae, I.W. Development of Infrared Ray Curing Technology at Continuous Coil Coating Line. In Proceedings of the Materials Science Forum 2010; Trans Tech Publications Ltd.: Bäch, Switzerland, 2010; pp. 1819–1822.
13. Véchot, L.; Bombard, I.; Laurent, P.; Lieto, J. Experimental and modelling study of the radiative curing of a polyester-based coating. *Int. J. Therm. Sci.* **2006**, *45*, 86–93. [CrossRef]
14. Choi, J.W.; Chun, W.P.; Oh, S.H.; Lee, K.J.; Kim, S.I. Experimental studies on a combined near infrared (NIR) curing system with a convective oven. *Prog. Org. Coat.* **2016**, *91*, 39–49. [CrossRef]

15. Mabbett, I.; Elvins, J.; Gowenlock, C.; Glover, C.; Jones, P.; Williams, G.; Worsley, D. Addition of carbon black NIR absorber to galvanised steel primer systems: Influence on NIR cure of polyester melamine topcoats and corrosion protection characteristics. *Prog. Org. Coat.* **2014**, *77*, 494–501. [CrossRef]
16. Ding, C.; Khir, R.; Pan, Z.; Wood, D.F.; Venkitasamy, C.; Tu, K.; El-Mashad, H.; Berrios, J. Influence of infrared drying on storage characteristics of brown rice. *Food Chem.* **2018**, *264*, 149–156. [CrossRef]
17. Ding, C.; Khir, R.; Pan, Z.; Zhao, L.; Tu, K.; El-Mashad, H.; Mchugh, T.H. Improvement in Shelf Life of Rough and Brown Rice Using Infrared Radiation Heating. *Food Bioprocess Technol.* **2015**, *8*, 1149–1159. [CrossRef]
18. Feng, Y.; Wu, B.; Yu, X.; Yagoub, A.E.A.; Sarpong, F.; Zhou, C. Effect of catalytic infrared dry-blanching on the processing and quality characteristics of garlic slices. *Food Chem.* **2018**, *266*, 309–316. [CrossRef]
19. Bröckerhoff, P.; Emonts, B. Use of natural gas in a catalytic radiant burner for low-emission heat production. In *Studies in Surface Science and Catalysis*; de Pontes, M., Espinoza, R.L., Nicolaides, C.P., Scholtz, J.H., Scurrell, M.S., Eds.; Elsevier: Amsterdam, The Netherlands, 1997; Volume 107, pp. 133–138.
20. Chen, J.; Arandiyan, H.; Gao, X.; Li, J. Recent Advances in Catalysts for Methane Combustion. *Catal. Surv. Asia* **2015**, *19*, 140–171. [CrossRef]
21. He, L.; Fan, Y.; Bellettre, J.; Yue, J.; Luo, L. A review on catalytic methane combustion at low temperatures: Catalysts, mechanisms, reaction conditions and reactor designs. *Renew. Sustain. Energy Rev.* **2020**, *119*, 109589. [CrossRef]
22. Pfefferle, L.D.; Pfefferle, W.C. Catalysis in Combustion. *Catal. Rev. Sci. Eng.* **1987**, *29*, 219–267. [CrossRef]
23. Pfefferle, W.C. Catalytically-Supported Thermal Combustion. U.S. Patent US 3928961, 30 December 1975.
24. Defraeye, T. Advanced computational modelling for drying processes—A review. *Appl. Energy* **2014**, *131*, 323–344. [CrossRef]
25. Niamsuwan, S.; Kittisupakorn, P.; Suwatthikul, A. Enhancement of energy efficiency in a paint curing oven via CFD approach: Case study in an air-conditioning plant. *Appl. Energy* **2015**, *156*, 465–477. [CrossRef]
26. Ture, S.A.; Chandramohan, V.P. Effect of radiation heat transfer in convective drying of cranberry: Numerical solutions of one and two dimensional heat and mass transfer and comparison of results. *Therm. Sci. Eng. Prog.* **2021**, *22*, 100837. [CrossRef]
27. Torres, S.S.; Bautista, E.H.; Patiño, M.A.G.; Ramírez, J.R.; Lagunas, L.L.M.; Barriada-Bernal, L.G.; Lamine, H. Numerical simulation of contact vacuum drying of potato slices. *Therm. Sci. Eng. Prog.* **2022**, *33*, 101382. [CrossRef]
28. Güneş, D.; Kükrer, E.; Yıldırım, C. Experimental and computational design improvement assessment of a household toast grill. *Therm. Sci. Eng. Prog.* **2020**, *19*, 100609. [CrossRef]
29. Bombard, I.; Laurent, P.; Lieto, J.; Jeandel, G. A model of the infrared cure of powder coatings based on surface absorptivities in-situ measurements. *JCT Res.* **2008**, *5*, 353–363. [CrossRef]
30. Marold, B.; Funke, W. Determination of the glass transition temperature at polymer surfaces from the temperature dependence of wetting. *Prog. Org. Coat.* **1994**, *23*, 287–297. [CrossRef]
31. Jain, D.; Pathare, P.B. Selection and Evaluation of Thin Layer Drying Models for Infrared Radiative and Convective Drying of Onion Slices. *Biosyst. Eng.* **2004**, *89*, 289–296. [CrossRef]
32. Joshi, R.; Baek, I.; Joshi, R.; Kim, M.S.; Cho, B.-K. Detection of fabricated eggs using Fourier transform infrared (FT-IR) spectroscopy coupled with multivariate classification techniques. *Infrared Phys. Technol.* **2022**, *123*, 104163. [CrossRef]
33. Calvez, I.; Davoudi, S.; Szczepanski, C.R.; Landry, V. Low-gloss UV-curable coatings: Light mechanisms, formulations and processes—A review. *Prog. Org. Coat.* **2022**, *171*, 107039. [CrossRef]
34. Stewart, A.L.; Carr, W.W.; Williamson, V.A. Characterization of infrared absorption by powder coatings on steel panels. *J. Coat. Technol.* **1999**, *71*, 71–84. [CrossRef]
35. Yan, X.; Wang, L. Preparation and Performance of a Waterborne UV/Al Low Infrared Emissivity Coating. *Appl. Sci.* **2020**, *10*, 6423. [CrossRef]
36. Lan, F.; Ding, R.; Tian, Z.; Zhang, H.; Huang, Y.; Xu, G.; Bao, J. Preparation and performance of polyester/epoxy/acrylic resin for low gloss powder coatings. *China Plast. Ind.* **2020**, *48*, 24–28. (In Chinese) [CrossRef]
37. Kögl, D. The curing of powder coatings using gaseous infrared heaters: An analytical model to assess the process thermal efficiency. *Int. J. Therm. Sci.* **2000**, *39*, 762–769.

Disclaimer/Publisher's Note: The statements, opinions and data contained in all publications are solely those of the individual author(s) and contributor(s) and not of MDPI and/or the editor(s). MDPI and/or the editor(s) disclaim responsibility for any injury to people or property resulting from any ideas, methods, instructions or products referred to in the content.